Alexandria Engineering Journal (2016) 55, 321–329

HOSTED BY

Alexandria University

Alexandria Engineering Journal

www.elsevier.com/locate/aej
www.sciencedirect.com

ORIGINAL ARTICLE

Non-Newtonian model study for blood flow through a tapered artery with a stenosis

Noreen Sher Akbar

DBS&H, CEME, National University of Sciences and Technology, Islamabad, Pakistan

Received 15 February 2015; revised 1 August 2015; accepted 17 September 2015
Available online 19 November 2015

KEYWORDS

Tangent hyperbolic fluid;
Blood flow;
Tapered artery;
Stenosis;
Analytical solution

Abstract The blood flow through a tapered artery with a stenosis is analyzed, assuming the blood as tangent hyperbolic fluid model. The resulting nonlinear implicit system of partial differential equations is solved analytically with the help of perturbation method. The expressions for shear stress, velocity, flow rate, wall shear stress and longitudinal impedance are obtained. The variations of power law index m, Weissenberg number We, shape of stenosis n and stenosis size δ are discussed different type of tapered arteries.

1. Introduction

Blood flow is now well known to the physiologists as one of the major mechanisms due to its applications in arterial mechanics. In particular, blood flows in arteries is an important field of research because arterial diseases are a major cause of death in most of western countries. In the recent past, several theoretical and experimental studies [1–5] have been carried out to analyze the arterial flow characteristics of blood. Chakravarty and Sannigrahi [6] developed a nonlinear mathematical analytically to study the flow characteristics of blood through an artery in the presence of multistenoses when it is subjected to whole body acceleration. The unsteady non-Newtonian blood flow and mass transfer in symmetric and non-symmetric stenotic arteries are numerically simulated by Valencia and Villanueva [7]. Effect of stenosis on solitary waves in arteries has been studied by Bakirtas and Demiray [8]. Myers and Capper [9] studied exponential taper in arteries, and an exact solution has been evaluated to see its effect on blood flow velocity waveforms and impedance. The pulsatile flow of blood through a catheterized artery is analyzed by Sankar [10], assumed the blood as a two-fluid model. As the seminal contribution to the study of shear thinning viscoelastic nature of blood, Thurston [11] developed an extended Maxwell model which is applicable to one-dimensional flow. Some researchers [12–18] investigated that for blood flowing through small vessels, there is erythrocyte-freeplasma (Newtonian) layer adjacent to the vessel wall and a core layer of a suspension of all erythrocytes (non-Newtonian). Further recent literature can be viewed through Refs. [20–25].

Motivated from the extensive literature available on blood flow through arteries, the purpose of the present investigation is to discuss the tangent hyperbolic fluid [19] model for blood flow through a tapered artery with mild stenosis. The governing equations along with the boundary conditions of stenosed symmetric artery have been solved by regular perturbation method. The expressions for velocity, resistance impedance, wall shear stress and shearing stress at the stenosis throat have

E-mail address: noreensher@yahoo.com

Peer review under responsibility of Faculty of Engineering, Alexandria University.

http://dx.doi.org/10.1016/j.aej.2015.09.010
1110-0168

been examined. The graphical behavior of different type of tapered arteries has been discussed at the end of the article.

2. Formulation of the problem

We are considering the cylindrical coordinates (r, θ, z) in which $(r = 0)$ as the axis of the symmetry of the tube. We are considering the flow of an incompressible hyperbolic tangent fluid of constant viscosity η_0 and density ρ in a tube having length L and take $\bar{u}$ and $\bar{w}$ are the velocity component in $\bar{r}$ and $\bar{z}$ direction respectively. The geometry of the stenosis which is assumed to be symmetric can be described as [4].

$$h(z) = d(z)\left[1 - \eta\left(b^{n-1}(z-a) - (z-a)^n\right)\right], \quad a \leqslant z \leqslant a+b, \quad = d(z), \quad \text{otherwise} \tag{1}$$

with

$$d(z) = d_0 + \xi z, \tag{2}$$

where $d(z)$ is the radius of the tapered arterial segment in the stenotic region, d_0 is the radius of the non-tapered artery in the non-stenotic region, ξ is the tapering parameter, b is the length of stenosis, $(n \geqslant 2)$ is a parameter determining the shape of the constriction profile and referred to as the shape parameter (the symmetric stenosis occurs for $n = 2$) and a indicates its location as shown in Fig. 1. The parameter η is given by

$$\eta = \frac{\delta^* n^{\frac{n}{n-1}}}{d_0 b^n (n-1)}, \tag{3}$$

where δ denotes the maximum height of the stenosis located at

$$z = a + \frac{b}{n^{\frac{n}{n-1}}}.$$

The equations governing the steady incompressible tangent hyperbolic fluid are given as

$$\frac{\partial \bar{u}}{\partial \bar{r}} + \frac{\bar{u}}{\bar{r}} + \frac{\partial \bar{w}}{\partial \bar{z}} = 0, \tag{4}$$

$$\rho\left(\bar{u}\frac{\partial}{\partial \bar{r}} + \bar{w}\frac{\partial}{\partial \bar{z}}\right)\bar{u} = -\frac{\partial \bar{p}}{\partial \bar{z}} + \frac{1}{\bar{r}}\frac{\partial}{\partial \bar{r}}(\bar{r}\bar{\tau}_{\bar{r}\bar{r}}) + \frac{\partial}{\partial \bar{z}}(\bar{\tau}_{\bar{r}\bar{z}}) - \frac{\bar{\tau}_{\bar{\theta}\bar{\theta}}}{\bar{r}}, \tag{5}$$

$$\rho\left(\bar{u}\frac{\partial}{\partial \bar{r}} + \bar{w}\frac{\partial}{\partial \bar{z}}\right)\bar{w} = -\frac{\partial \bar{p}}{\partial \bar{z}} + \frac{1}{\bar{r}}\frac{\partial}{\partial \bar{r}}(\bar{r}\bar{\tau}_{\bar{r}\bar{z}}) + \frac{\partial}{\partial \bar{z}}(\bar{\tau}_{\bar{z}\bar{z}}). \tag{6}$$

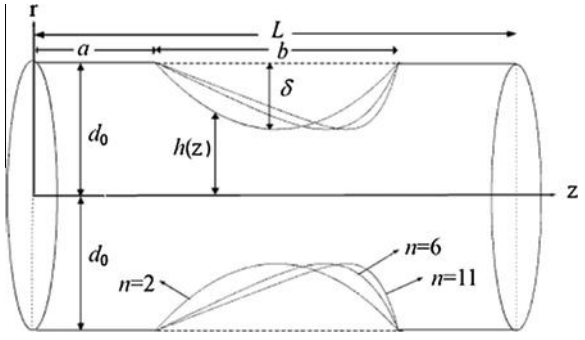

Figure 1 Geometry of the stenosis in the artery.

The constitutive equation for tangent hyperbolic fluid is defined as [19]

$$\widetilde{\mathbf{S}} = -P\mathbf{I} + \bar{\boldsymbol{\tau}}, \tag{7a}$$

$$\bar{\boldsymbol{\tau}} = \left[\left[\eta_\infty + (\eta_0 + \eta_\infty)\tanh\left(\Gamma\bar{\dot{\gamma}}\right)^m\right]\bar{\dot{\gamma}}\right], \tag{7b}$$

in which $\bar{\boldsymbol{\tau}}$ is the extra stress tensor, η_∞ is the infinite shear rate viscosity, η_0 is the zero shear rate viscosity, Γ is the time constant, m is the power law index and $\bar{\dot{\gamma}}$ is defined as

$$\bar{\dot{\gamma}} = \sqrt{\frac{1}{2}\sum_i\sum_j \bar{\dot{\gamma}}_{ij}\bar{\dot{\gamma}}_{ji}} = \sqrt{\frac{1}{2}\Pi}, \tag{8}$$

where $\Pi = \frac{1}{2}trac\left(\text{grad } V + (\text{grad } V)^T\right)^2$. Here Π is the second invariant strain tensor. We consider the constitution Eq. (7), the case for which $\eta_\infty = 0$ because we cannot find the solution at the infinite shear rate viscosity. The component of extra stress tensor therefore, can be written as

$$\bar{\boldsymbol{\tau}} = \eta_0\left[\left(\Gamma\bar{\dot{\gamma}}\right)^m\right]\bar{\dot{\gamma}} = \eta_0\left[\left(1 + \Gamma\bar{\dot{\gamma}} - 1\right)^m\right]\bar{\dot{\gamma}} = \eta_0\left[1 + m(\Gamma\bar{\dot{\gamma}} - 1)\right]\bar{\dot{\gamma}}. \tag{9}$$

Defining the non-dimensional variables

$$r = \frac{\bar{r}}{d_0},\quad z = \frac{\bar{z}}{b},\quad w = \frac{\bar{w}}{u_0},\quad u = \frac{b\bar{u}}{u_0\delta},\quad p = \frac{d_0^2\bar{p}}{u_0 b\eta_0},\quad h = \frac{\bar{h}}{d_0},\quad We = \frac{\Gamma u_0}{d_0},$$
$$Re = \frac{\rho b u_0}{\eta_0},\quad \widetilde{\mathbf{S}}_{rr} = \frac{b\bar{\tau}_{rr}}{u_0\eta_0},\quad \widetilde{\mathbf{S}}_{rz} = \frac{d_0\bar{\tau}_{rz}}{u_0\eta_0},\quad \widetilde{\mathbf{S}}_{zz} = \frac{b\bar{\tau}_{zz}}{u_0\eta_0},\quad \widetilde{\mathbf{S}}_{\theta\theta} = \frac{b\bar{\tau}_{\theta\theta}}{u_0\eta_0}, \tag{10}$$

where u_0 is the velocity averaged over the section of the tube of the width d_0.

Making use of Eqs. (9) and (10) into Eqs. (4)–(6), the appropriate equations describing the steady flow of an incompressible tangent hyperbolic fluid in the case of mild stenosis $\left(\frac{\delta^*}{d_0} \ll 1\right)$, subject to the additional conditions [4]

$$\text{(i)} \quad \frac{Re\,\delta^* n^{\left(\frac{1}{n-1}\right)}}{b} \ll 1, \tag{11}$$

$$\text{(ii)} \quad \frac{d_0 n^{\left(\frac{1}{n-1}\right)}}{b} \sim O(1), \tag{12}$$

can be written as

$$\frac{\partial u}{\partial r} + \frac{u}{r} + \frac{\partial w}{\partial z} = 0, \tag{13}$$

$$\frac{\partial p}{\partial r} = 0, \tag{14}$$

$$\frac{\partial p}{\partial z} = \frac{1}{r}\frac{\partial}{\partial r}\left[r\left((m-1)\left(\frac{\partial w}{\partial r}\right) + Wem\left(\frac{\partial w}{\partial r}\right)^2\right)\right]. \tag{15}$$

The corresponding boundary conditions are

$$\frac{\partial w}{\partial r} = 0 \quad \text{at } r = 0, \tag{15a}$$

$$w = 0 \quad \text{at } r = h(z), \tag{15b}$$

where

$$h(z) = (1 + \xi z)[1 - \eta_1((z-\sigma) - (z-\sigma)^n)], \quad \sigma \leqslant z \leqslant \sigma + 1, \tag{16}$$

and

$$\eta_1 = \frac{\delta n^{\frac{n}{n-1}}}{(n-1)}, \quad \delta = \frac{\delta^*}{d_0}, \quad \sigma = \frac{a}{b}, \quad \xi' = \frac{\xi b}{d_0}, \tag{17}$$

where $(\xi = \tan\phi)$, ϕ is called tapered angle and for converging tapering $(\phi < 0)$, non-tapered artery $(\phi = 0)$ and the diverging tapering $(\phi > 0)$ (as shown in Fig. 2).

3. Solution of the problem

3.1. Perturbation solution

To get the perturbation solution we expand w, p and Q by taking We as a perturbation parameter as follows

$$w = w_0 + Wew_1 + O(We)^2, \tag{18}$$

$$p = p_0 + Wep_1 + O(We)^2, \tag{19}$$

$$Q = Q_0 + WeQ_1 + O\left(We^2\right)^2. \tag{20}$$

With the help of Eqs. (18)–(20), the solutions for velocity field and pressure gradient for small We can be written as follows

$$w(r,z) = \frac{dp}{dz}\left(\frac{r^2 - h^2}{4}\right) - We\left(\frac{64Q^2m\left(r^3 - h^3\right)}{3(1-m)h^8}\right), \tag{21}$$

$$\frac{dp}{dz} = -\frac{16Q(1-m)}{h^4} + We\left(\frac{512mQ^2}{5h^7}\right). \tag{22}$$

The pressure drop $(\Delta p = p$ at $z = 0$ and $\Delta p = -p$ at $z = L)$ across the stenosis between the section $z = 0$ and $z = L$ is obtained from (22) as done by [4]

$$\Delta p = \int_0^L \left(-\frac{dp}{dz}\right) dz. \tag{23}$$

3.2. Resistance impedance

With the help of Eq. (23), the resistance impedance is defined as

$$\tilde{\lambda} = \frac{\Delta p}{Q} = 4\left\{\int_0^a F(z)|_{h=1} dz + \int_a^{a+b} F(z)dz + \int_{a+b}^L F(z)|_{h=1} dz\right\}, \tag{24}$$

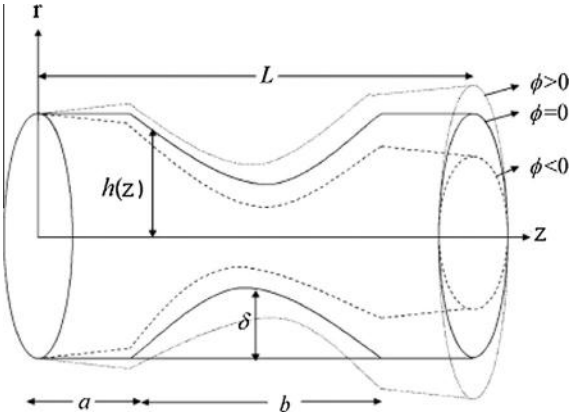

Figure 2 Geometry of the axially stenosed tapered artery for different tapered angle.

where

$$F(z) = \frac{4(1-m)}{h^4} - We\left(\frac{128mQ}{5h^7}\right), \tag{25}$$

Eq. (24) gives

$$\tilde{\lambda} = \left\{(L-b)\left(4(1-m) - We\left(\frac{128mQ}{5}\right)\right) + \int_a^{a+b} F(z)dz\right\}. \tag{26}$$

3.3. Expression for the wall shear stress

The nonzero dimensionless shear stress is given by

$$\widetilde{\mathbf{S}}_{rz} = \left[\left(\frac{\partial w}{\partial r}\right)(1-m) + Wem\left(\frac{\partial w}{\partial r}\right)^2\right]. \tag{27}$$

The expression for wall shear stress can be calculated as

$$\widetilde{\mathbf{S}}_{rz} = \left[\left(\frac{\partial w}{\partial r}\right)(1-m) + Wem\left(\frac{\partial w}{\partial r}\right)^2\right]\Bigg|_{r=h}. \tag{28}$$

Invoking Eq. (21) into (28), we obtain

$$\widetilde{\mathbf{S}}_{rz} = \left[4Q(1-m)R(z) + 16WemQ^2(R(z))^2\right], \tag{29}$$

where

$$R(z) = -\frac{F(z)h}{2(1-m)} - \frac{16WemQ}{(1-m)h^6}.$$

The shearing stress at the stenosis throat i.e. the wall shear at the maximum height of the stenosis located at $z = \frac{a}{b} + \frac{1}{n^{\frac{n}{n-1}}}$ i.e. $\tilde{\tau}_s = \widetilde{\mathbf{S}}_{rz}\big|_{h=1-\delta}$ is defined as

$$\tilde{\tau}_s = \left[4Q(1-m)J + 16WemQ^2(J)^2\right], \tag{30}$$

where

$$J = -\frac{K(1-\delta)}{2(1-m)} - \frac{16WemQ}{(1-m)(1-\delta)^6},$$

$$K = \frac{4(1-m)}{(1-\delta)^4} - We\left(\frac{128mQ}{5(1-\delta)^7}\right). \tag{31}$$

The final expression for the dimensionless resistance to λ, wall shear stress $\mathbf{S}_{rz}$ and the shearing stress at the throat τ_s by

$$\lambda = \frac{1}{3}\left\{\left(1 - \frac{b}{L}\right)\left(4(1-m) - We\left(\frac{128mQ}{5}\right)\right) + \frac{1}{L}\int_a^{a+b} F(z)dz\right\}, \tag{32}$$

$$\mathbf{S}_{rz} = \left[(1-m)R(z) + 4WemQ(R(z))^2\right], \tag{33}$$

$$\tau_s = \left[(1-m)J + 4WemQ(J)^2\right], \tag{34}$$

where

$$\lambda = \frac{\tilde{\lambda}}{\lambda_0}, \quad \mathbf{S}_{rz} = \frac{\widetilde{\mathbf{S}}_{rz}}{\tau_0}, \quad \tau_s = \frac{\tilde{\tau}_s}{\tau_0}, \quad \lambda_0 = 3L, \quad \tau_0 = 4Q.$$

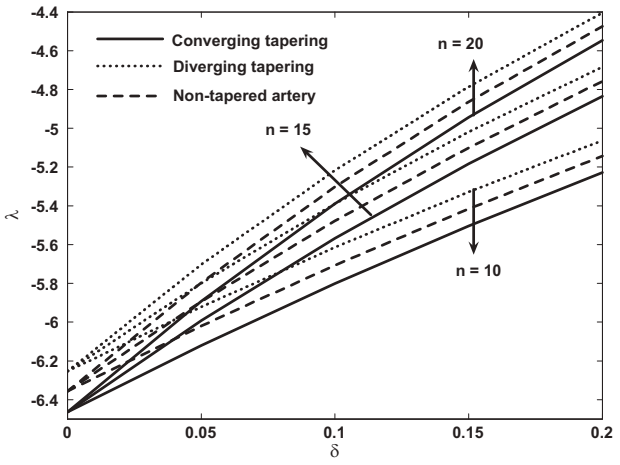

Figure 3 Variation of resistance for $Q = 0.9,\ We = 0.1,\ b = 1,\ \sigma = 0.0,\ L = 1,\ m = 2,\ z = .95$.

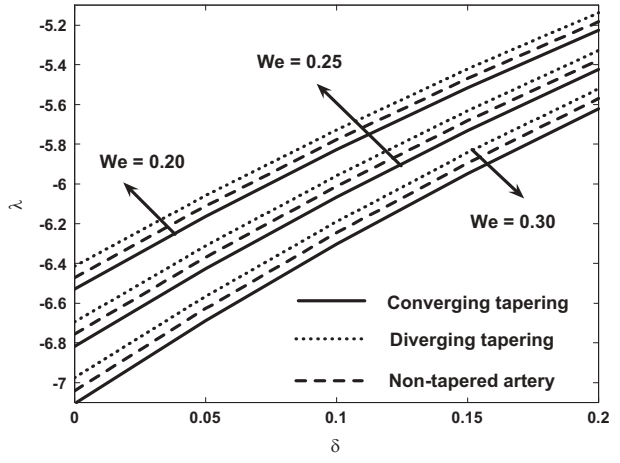

Figure 4 Variation of resistance for $Q = 0.5,\ n = 2,\ b = 1,\ \sigma = 0.0,\ L = 1,\ m = 2,\ z = .85$.

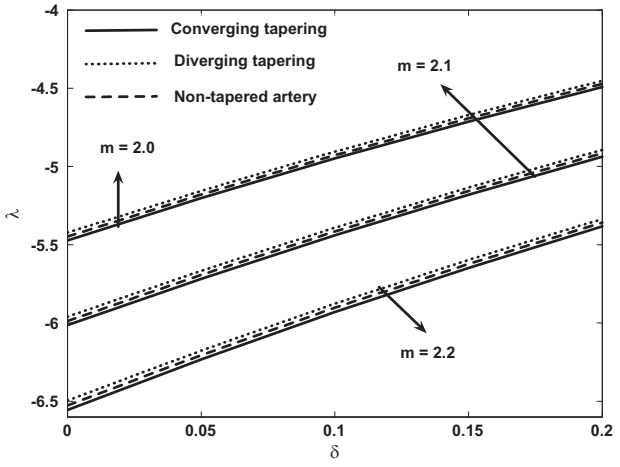

Figure 5 Variation of resistance for $Q = 0.1,\ We = 0.1,\ b = 1,\ \sigma = 0.0,\ L = 1,\ \delta = 0.2,\ z = .85,\ n = 2$.

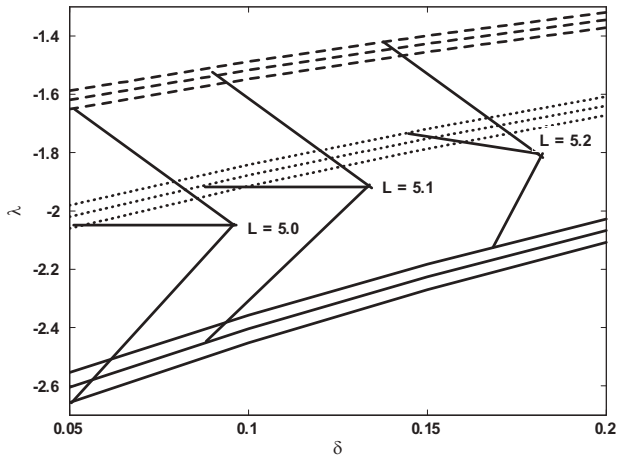

Figure 6 Variation of resistance for $Q = 0.1,\ We = 0.1,\ b = 1,\ \sigma = 0.0,\ m = 2,\ n = 2,\ \delta = 0.2,\ z = .85$.

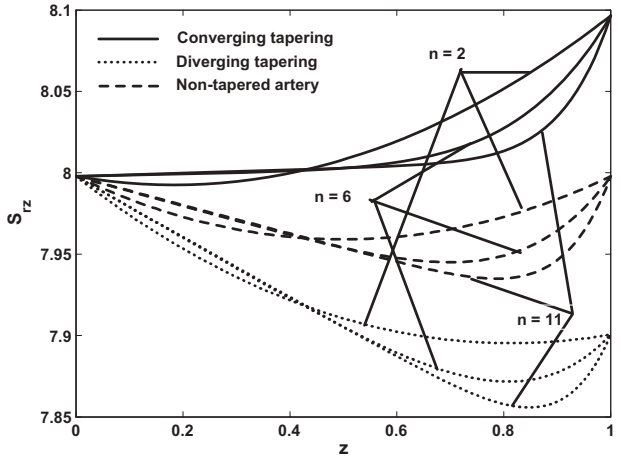

Figure 7 Variation of wall stress for $Q = 0.02,\ We = 0.5,\ \sigma = 0.0,\ \delta = 0.002,\ m = 5$.

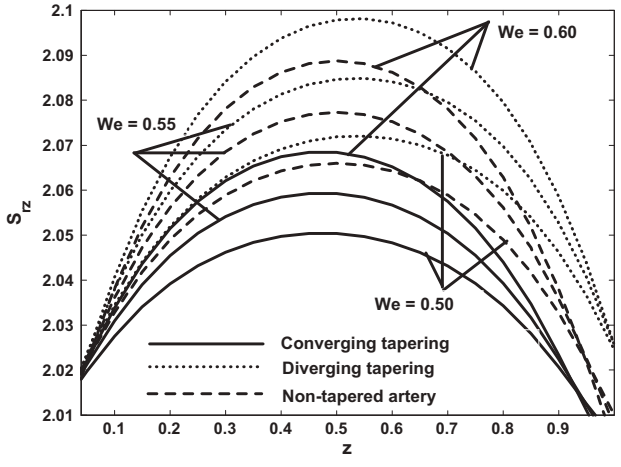

Figure 8 Variation of wall stress for $Q = 0.02,\ \sigma = 0.0,\ \delta = 0.002,\ n = 2,\ m = 5$.

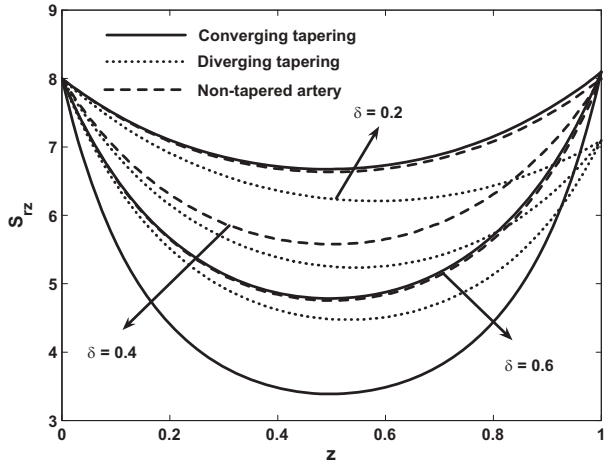

Figure 9 Variation of wall stress for $Q = 0.02,\ We = 0.5,\ \sigma = 0.0,\ n = 2,\ m = 5.$

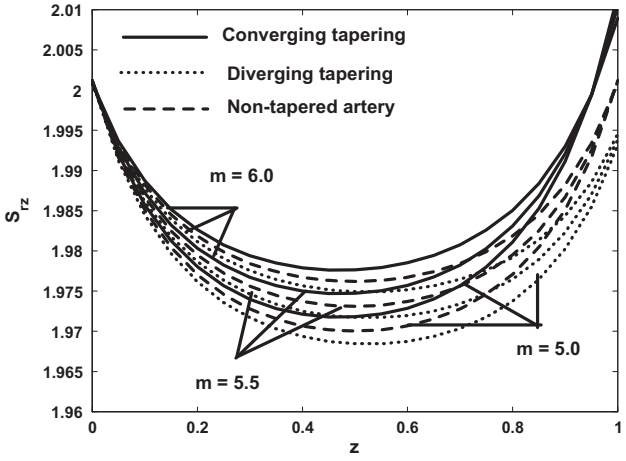

Figure 10 Variation of wall stress for $Q = 0.5,\ We = 0.5,\ \sigma = 0.0,\ \delta = 0.002,\ n = 2.$

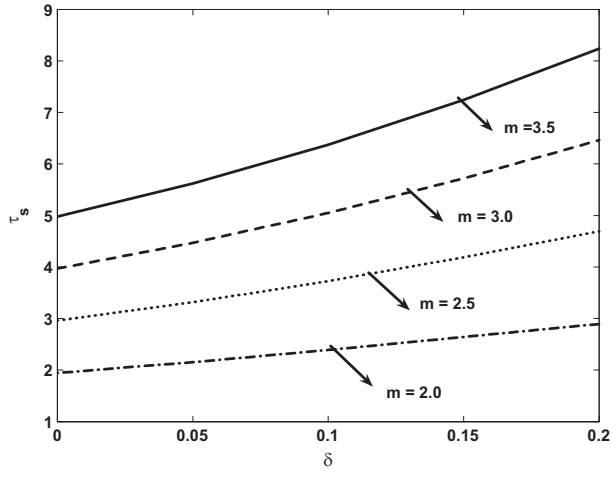

Figure 11 Variation of shear stress at the stenosis throat for $Q = 0.02,\ We = 0.5.$

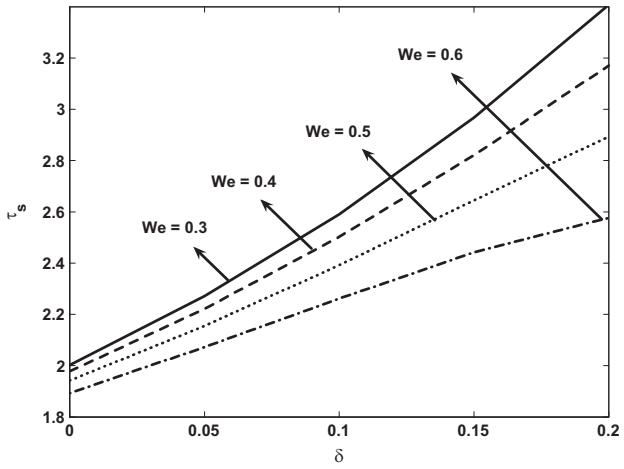

Figure 12 Variation of shear stress at the stenosis throat for $Q = 0.02,\ m = 2.$

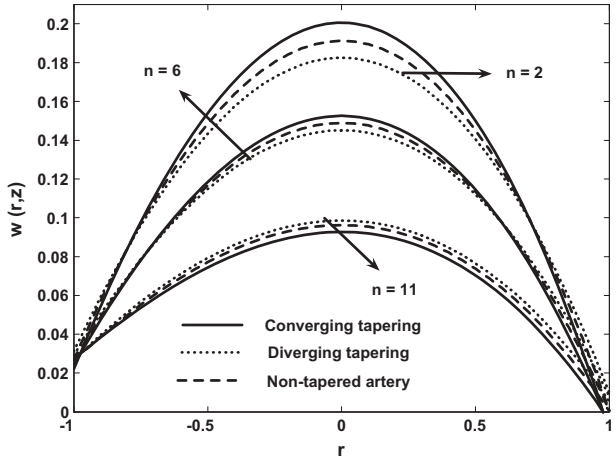

Figure 13 Variation of velocity profile for $Q = 0.05,\ We = 0.5,\ m = 3,\ \delta = 0.05,\ z = .5,\ \sigma = 0.00.$

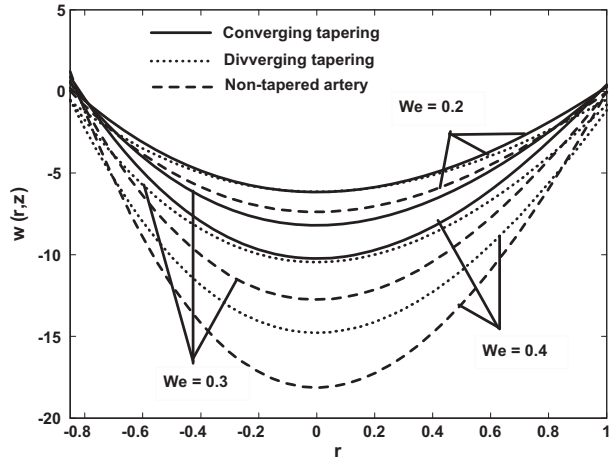

Figure 14 Variation of velocity profile for $Q = -0.5,\ n = 11,\ m = 2,\ \delta = 0.05,\ z = 0.5,\ \sigma = 0.00.$

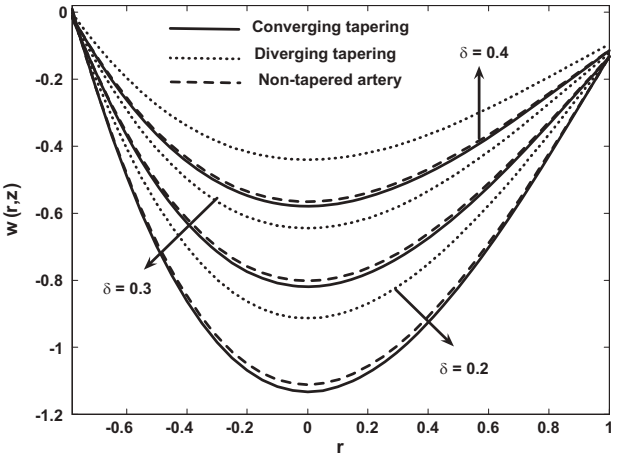

Figure 15 Variation of velocity profile for $Q = 0.3,\ n = 11,\ m = 2,\ z = 0.5,\ \sigma = 0.00,\ We = 0.5.$

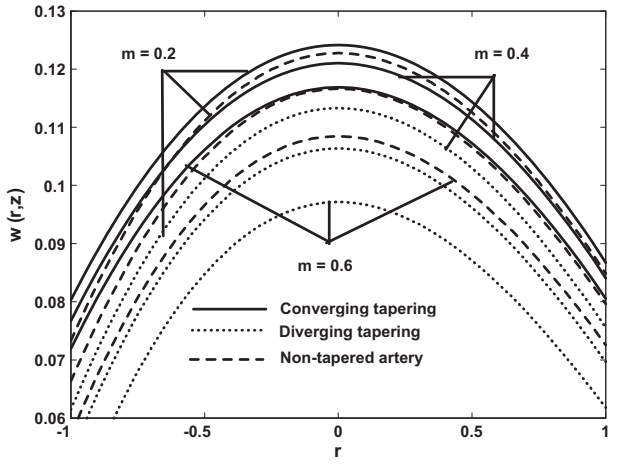

Figure 16 Variation of velocity profile for $Q = 0.3,\ n = 11,\ \delta = 0.002,\ z = 0.5,\ \sigma = 0.00,\ We = 0.5.$

4. Graphical results and discussion

The quantitative effects of the power law index m, Weissenberg number We, the stenosis shape n and maximum height of the stenosis δ for converging tapering, diverging tapering and non-tapered arteries for tangent hyperbolic fluid are observed physically through Figs. 3–15. Figs. 3–6 are prepared to see the variation of shear stress for different parameters of interest, and we notice that the impedance resistance increases for converging tapering, diverging tapering and non-tapered arteries when we increase n and L while decreases with the increase of We and m. We also observed that resistive impedance in a diverging tapering appears to be smaller than those in converging tapering because the flow rate is higher in the former than that in the latter, as anticipated and impedance resistance attains its maximum values in the symmetric stenosis case $(n = 2)$. Figs. 7–10 show how the converging tapering, diverging tapering and non-tapered arteries influence on the wall shear stress S_{rz}. It is observed that with an increase in m and We shear stress increases while decreases with an increase in δ and n, the stress yield diverging tapering with tapered angle $\phi > 0$, converging tapering with tapered angle $\phi < 0$ and non-tapered artery with tapered angle $\phi = 0$. Figs. 11 and 12 are prepared to see the variation of the shearing stress at the stenosis throat τ_s with δ. It is analyzed through figures that shearing stress at the stenosis throat increases with an increase in m and decreases with an increase in We. It can also be depict that shearing stress at the throat τ_s possess an inverse variation to the flow resistance λ with respect to power law index m, Weissenberg number We. Finally the variation of axial velocity for m, We, δ and n for the case of a converging tapering, diverging tapering and non-tapered arteries is displayed in Figs. 13–16. From Figs. 13–16 we observed that with an increase in We, m and n velocity profile decreases while increases with an increase in δ. It is also seen that for the case of converging tapering velocity gives larger values as compared to the case of diverging tapering and non-tapered arteries. Trapping phenomena have been discussed through Figs. 17–20. Fig. 17 shows the stream lines for different values of the power law index m. It is observed that with an increase in m size of the

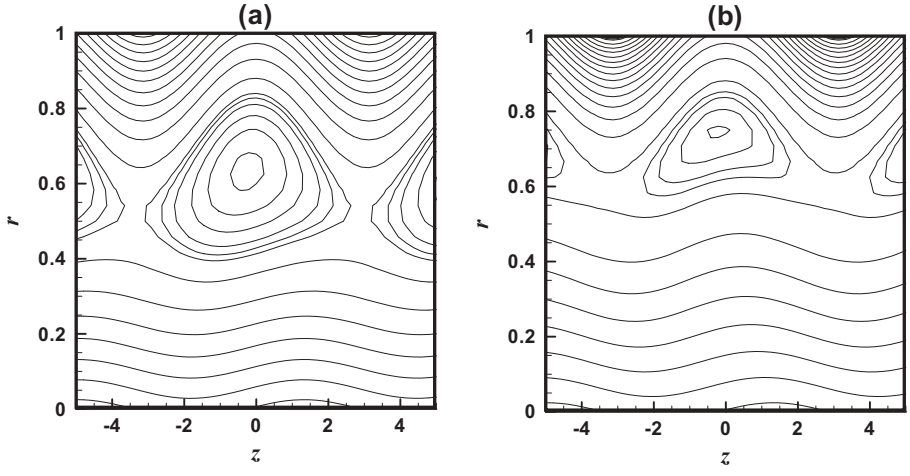

Figure 17 Stream lines for different values of m (a) $m = 7$ and (b) $m = 9$ other parameters are $\phi = \pi,\ Q = 0.01,\ We = 0.2,\ \sigma = 0.2,\ \delta = 0.8,\ n = 7.$

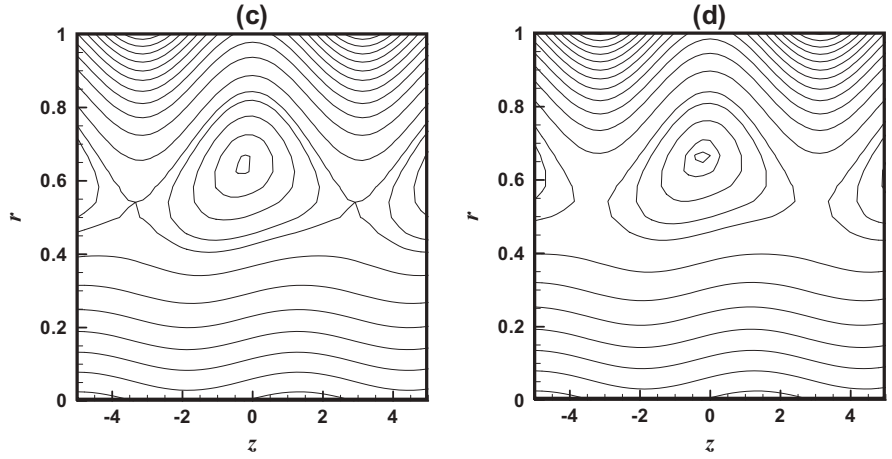

Figure 18 Stream lines for different values of n (c) $n = 6$ and (d) $n = 9$ other parameters are $\phi = \pi,\ Q = 0.01,\ We = 0.2,\ \sigma = 0.2,\ \delta = 0.8,\ m = 7$.

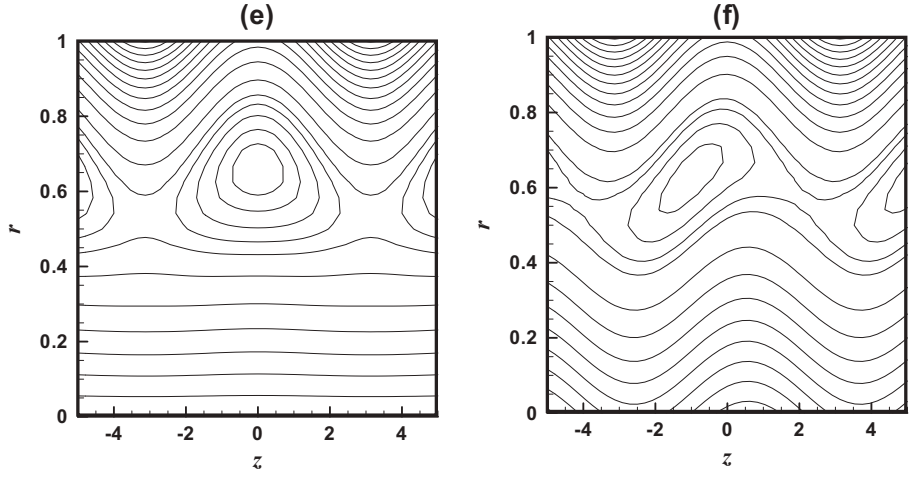

Figure 19 Stream lines for different values of δ (e) $\delta = 0.6$ and (f) $\delta = 0.9$ other parameters are $\phi = \pi,\ Q = 0.01,\ We = 0.2,\ \sigma = 0.2,\ m = 7,\ n = 6$.

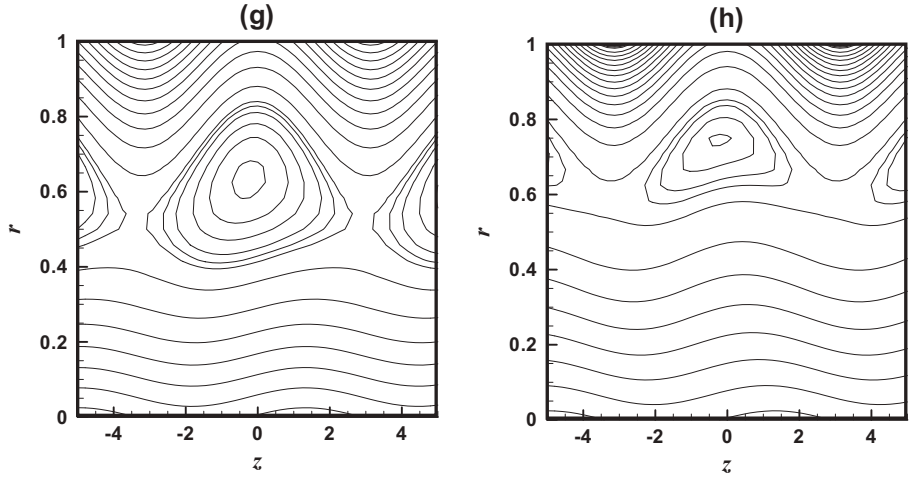

Figure 20 Stream lines for different values of We (g) $We = 0.2$ and (h) $We = 0.5$ other parameters are $\phi = \pi,\ Q = 0.01,\ \delta = 0.5,\ \sigma = 0.2,\ m = 7,\ n = 6$.

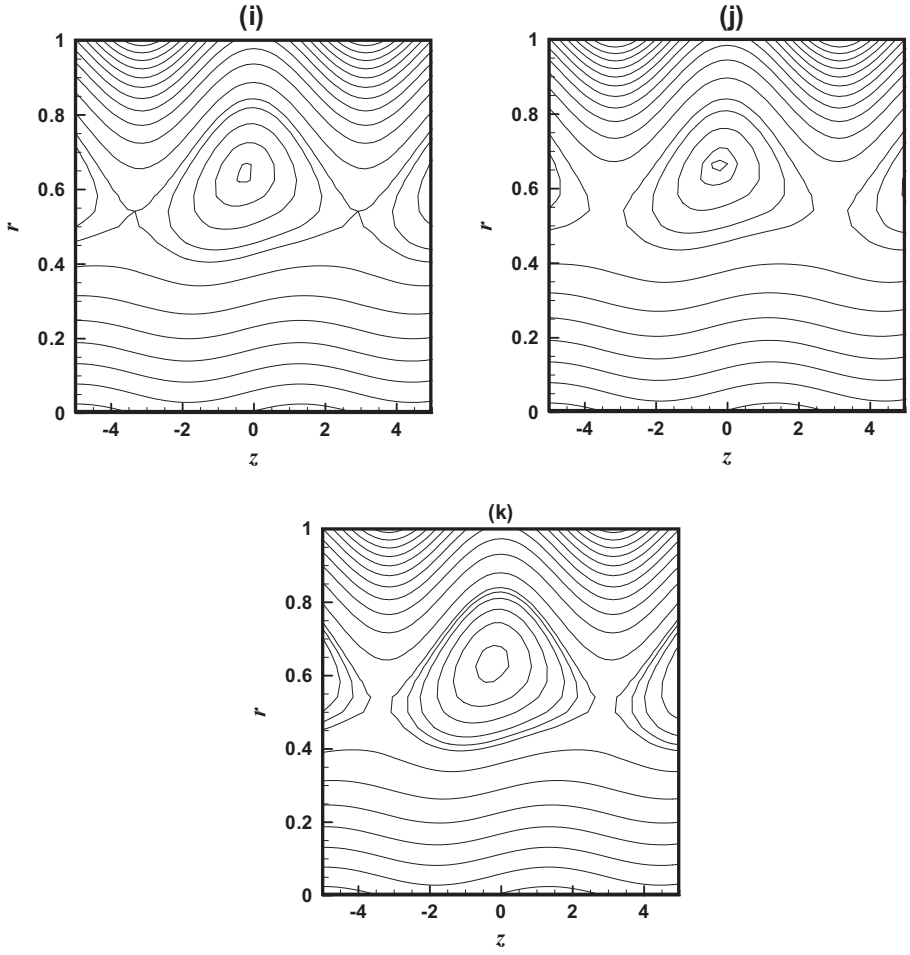

Figure 21 Stream lines for different values of tapered angle ϕ (i) $\phi = -0.2$, (j) $\phi = 0.0$ and (k) $\phi = 0.2$ other parameters are $We = 0.3,\ Q = 0.01,\ \delta = 0.5,\ \sigma = 0.2,\ m = 7,\ n = 6$.

trapping bolus increases but the number of trapping bolus decreases. Stream lines for different values of the stenosis shape n are prepared in Fig. 18. It is analyzed that the size of the trapping bolus increases when we increase the n. Figs. 19 and 20 are plotted to see the stream lines for different values of height of the stenosis δ and Weissenberg number We. It is seen that the size and number of the trapping bolus increase with an increases in height of the stenosis δ and the size of the trapping bolus increases while number of tapping bolus decreases with an increase in the Weissenberg number We. Fig. 21 shows the streamlines for tapered angle ϕ. It is seen that the number of trapped bolus and size of trapped bolus increases for the case of the diverging tapering ($\phi > 0$) as compared to converging tapering ($\phi < 0$), and non-tapered artery ($\phi = 0$).

References

[1] Biyue Liu, Dalin Tang, A numerical simulation of viscous flows in collapsible tubes with stenoses, Appl. Numer. Math. 32 (2000) 87–101.
[2] S.C. Ling, H.B. Atabek, A nonlinear analysis of pulsatile blood flow in arteries, J. Fluid Mech. 55 (1972) 492–511.
[3] Kh.S. Mekheimer, M.A. El Kot, Influence of magnetic field and Hall currents on blood flow through a stenotic artery, Appl. Math. Mech. 29 (2008) 1093–1104.
[4] Kh.S. Mekheimer, M.A. El Kot, The micropolar fluid model for blood flow through a tapered artery with a stenosis, Acta Mech. Sin. 24 (2008) 637–644.
[5] J.C. Misra, G.C. Shit, Effect of magnetic field on blood flow through an artery: a numerical model, Tom 12 (4) (2007).
[6] S. Chakravarty, A.K.R. Sannigrahi, A nonlinear mathematical model of blood flow in a constricted artery experiencing body acceleration, Math. Comput. Model. 29 (1999) 9–25.
[7] A. Valencia, M. Villanueva, Unsteady flow and mass transfer in models of stenotic arteries considering fluid–structure interaction, Int. Commun. Heat Mass Transfer 33 (2006) 966–975.
[8] I. Bakirtas, H. Demiray, Amplitude modulation of nonlinear waves in a fluid-filled tapered elastic tube, Appl. Math. Comput. 154 (2004) 747–767.
[9] L.J. Myers, W.L. Capper, Exponential taper in arteries: an exact solution of its effect on blood flow velocity wave forms and impedance, Med. Eng. Phys. 26 (2004) 147–155.
[10] D.S. Sankar, A two-fluid model for pulsatile flow in catheterized blood vessels, Int. J. Non-linear Mech. 44 (2009) 337–351.
[11] G.B. Thurston, Rheological parameters for the viscosity, viscoelasticity and thixotropy of blood, Biorheology 16 (1979) 149–162.
[12] G. Bugliarello, J. Sevilla, Velocity distribution and other characteristics of steady and pulsatile blood flow in fine glass tubes, Biorheology 7 (1970) 85–107.
[13] G.B. Thurston, Plasma release-cell layering theory for blood flow, Biorheology 26 (1989) 199–214.

[14] S. Chakravarthy, S. Sarifuddin, P.K. Mandal, Unsteady flow of a two-layer blood stream pasta tapered flexible artery under stenotic conditions, Comput. Methods Appl. Math. 4 (2004) 391–409.
[15] Kh.S. Mekheimer, M.A. El Kot, The micropolar fluid model for blood flow through a stenotic arteries, Int. J. Pure Appl. Math. 36 (2007) 393–405.
[16] Kh.S. Mekheimer, M.A. El Kot, Suspension model for blood flow through arterial catheterization, Chem. Eng. Commun. 197 (2010) 1195–1214.
[17] Kh.S. Mekheimer, M.A. El Kot, Mathematical modelling of unsteady flow of a Sisko fluid through an anisotropically tapered elastic arteries with time-variant overlapping stenosis, Appl. Math. Model. 36 (2012) 5393–5407.
[18] Noreen Sher Akbar, S. Nadeem, Changhoon Lee, Biomechanical analysis of Eyring Prandtl fluid model for blood flow in stenosed arteries, Int. J. Nonlinear Sci. Numer. Simul. 14 (2013) 345–353.
[19] S. Nadeem, Noreen Sher Akbar, Series solutions for the peristaltic flow of a tangent hyperbolic fluid in a uniform inclined tube, Z. Naturforsch. 65a (2010) 887–895.
[20] Osnat Eytan, Ariel J. Jaffa, David Elad, Peristaltic flow in a tapered channel: application to embryo transport within the uterine cavity, Med. Eng. Phys. 23 (7) (2001) 473–482.
[21] M. Kothandapani, J. Prakash, V. Pushparaj, Analysis of heat and mass transfer on MHD peristaltic flow through a tapered asymmetric channel, J. Fluid 2015 (2015), 9pages 561263.
[22] M. Kothandapani, J. Prakash, Effect of radiation and magnetic field on peristaltic transport of nanofluids through a porous space in a tapered asymmetric channel, J. Magn. Magn. Mater. 378 (2015) 152–163.
[23] M. Kothandapani, J. Prakash, The peristaltic transport of Carreau Nanofluids under effect of a magnetic field in a tapered asymmetric channel: application of the cancer therapy, J. Mech. Med. Bio. (2014).
[24] M. Kothandapani, J. Prakash, Peristaltic transport of a MHD Carreau fluid in a tapered asymmetric channel with permeable walls, Int. J. Biomath. 15 (2015) 1550030, 32pages.
[25] M. Kothandapani, J. Prakash, Influence of heat source, thermal radiation and inclined magnetic field on peristaltic flow of a Hyperbolic tangent nanofluid in a tapered asymmetric channel, IEEE Trans. Nanobiosci. 14 (2015) 385–392.